Maximum entropy modeling of oxygen vibrational excitation and dissociation

Jiaao Hao* and Chih-Yung Wen†
Department of Mechanical Engineering, The Hong Kong Polytechnic University, Kowloon, Hong Kong

(Received 20 June 2018; published 13 May 2019)

The vibrational excitation and dissociation of oxygen are modeled using different approaches with a range of fidelity, including the conventional two-temperature model, the state-specific method, and two variations of a model based on the maximum entropy principle. Comparison of the post-shock predictions with recent shock tube experimental data shows that the maximum entropy quadratic model predicts similar trends to the state-specific method and the experimental data. Although the maximum entropy quadratic model has significantly fewer equations than the state-specific method, no gain in computational efficiency is seen. Hence, the former model is further simplified by assuming that the vibrational relaxation can be described by the Landau-Teller formulation, with the corresponding relaxation times for O_2-O_2 and O_2-O interactions determined from state-specific calculations of relaxation in a heat bath. The post-shock simulations indicate that the modified maximum entropy quadratic model maintains sufficient prediction accuracy while significantly improving computational efficiency. The proposed model could be used in computational fluid dynamics solvers for hypersonic nonequilibrium flow simulations.

DOI: 10.1103/PhysRevFluids.4.053401

I. INTRODUCTION

Thermochemical nonequilibrium phenomena are frequently encountered during hypersonic flights. Across the strong shock wave generated by a hypersonic vehicle, a large amount of kinetic energy in the freestream is converted into molecular or atomic translational energy. The internal energy modes of the fluid are excited at a finite rate due to the high translational temperature. Meanwhile, chemical reactions including dissociation, neutral exchange, and ionization can occur among reactive species. In most circumstances, thermal nonequilibrium and chemical reactions are coupled. For instance, the vibrational energy level populations of molecules affect the dissociation rates and dissociation, in turn, causes the removal of vibrational energy, which is commonly referred to as vibration-dissociation coupling effects. Such effects dominate the flowfields around hypersonic vehicles at relatively low velocities, such as capsules reentering from low Earth orbit and hypersonic cruisers. Further developments in hypersonic flight technologies will require an accurate modeling of this phenomenon.

The two-temperature (2-T) model is perhaps the most widely used approach to describe vibrational excitation and dissociation. It is commonly assumed that the vibrational mode of molecules relaxes according to the Landau-Teller theory [1]. Various models (Park [2], Hansen [3], Marrone–Treanor [4], Hammerling [5], Macheret-Fridman [6], etc.) have been proposed in the past several decades to calculate the nonequilibrium rate coefficients and the vibrational energy added or removed due to recombination and dissociation. Benefiting from a simple description of the internal energy level populations with a vibrational temperature, these models have been partly successful at hypersonic nonequilibrium simulation. However, the highly empirical assumptions and

*jiaao.hao@polyu.edu.hk
†cywen@polyu.edu.hk

parameters involved in the 2-T model inevitably introduce modeling errors, especially for strongly nonequilibrium flows.

Recent advances in computational resources have promoted the use of high-fidelity modeling, namely, the state-specific method. This approach traces the temporal and spatial variation of each vibrational level by solving a system of master equations and thus represents the complete description of the nonequilibrium state of the gas. However, it requires the solution of substantially more equations. The memory access to large data sets of kinetic rate coefficients is also expensive. Consequently, detailed state-specific simulations have been applied only to one-dimensional and two-dimensional inviscid flows [7–9].

To reduce the computational expense, a new method termed the "coarse-grained model" [10–14] has been proposed, in which the internal levels are divided into groups and the level populations in each group are reconstructed based on the maximum entropy (ME) principle [15]. In the literature, the ME principle has been applied to model vibration-dissociation coupling for computational fluid dynamics (CFD) [16], direct simulation Monte Carlo (DSMC) [17,18], and state-specific simulations [19,20]. Most of these studies adopted the ME approach to interpret state-specific cross sections and build reduced models of vibrational relaxation and dissociation. This approach was recently generalized in Refs. [10–14] to express the logarithm of the vibrational distribution profile as either a linear or quadratic function to capture the non-Boltzmann behaviors. Heat bath calculations for N_2-N interactions have shown that the process of vibrational excitation and dissociation could be captured accurately with only a few groups. Such a method is very promising for CFD applications.

This study aims to reproduce the complete process of vibrational excitation and dissociation of oxygen behind a normal shock wave using the ME linear and quadratic models and to compare the predictions with high-fidelity state-specific results and recent shock tube experimental data. Notably, O_2-O_2 interactions are considered in this study, which also aims to further simplify the ME quadratic model to reduce the computational expense. A model suitable for incorporation in CFD solvers is established.

II. THERMOCHEMICAL NONEQUILIBRIUM MODELS

In this section, various models of the vibrational excitation and dissociation of oxygen are presented, including a conventional 2-T model, two improved models based on ME principles, and a high-fidelity state-specific method. For all models, it is assumed that the rotational energy mode of molecular oxygen is fully excited and in equilibrium with the translational mode, corresponding to a translational-rotational temperature T_{tr}. In addition, only the ground electronic state is considered. These assumptions generally hold at temperatures below 10 000 K [21]. The thermochemical nonequilibrium flow downstream of a normal shock wave is governed by the one-dimensional compressible flow equations, comprising the conservation equations of species mass, mixture momentum, and total energy. Additional equations related to the vibrational energy modes are included in the 2-T and ME models.

A. Conventional two-temperature model

Under the conventional 2-T assumption, molecular oxygen is treated as a harmonic oscillator relaxing via the Boltzmann distribution in terms of a vibrational temperature T_{v}. The corresponding governing equations can be expressed as

$$\frac{\partial}{\partial x}(\rho_s u) = \omega_s, \quad s = 1, 2,$$

$$\frac{\partial}{\partial x}(\rho u^2 + p) = 0,$$

$$\frac{\partial}{\partial x}\left[\rho u\left(h+\frac{1}{2}u^2\right)\right]=0,$$
$$\frac{\partial}{\partial x}(\rho u e_{\mathrm{v}})=\omega_{\mathrm{v}}, \tag{1}$$

where ρ_s is the density of species s; ρ, u, p, h, and e_{v} are the mixture density, velocity, pressure, enthalpy, and vibrational energy, respectively; ω_s is the mass production rate of species s due to chemical reactions; and ω_{v} is the source term of the vibrational energy equation.

According to the law of mass action, ω_s can be readily obtained for O_2 and O as follows:

$$\frac{N_{\mathrm{Av}}}{M_{\mathrm{O_2}}}\omega_{\mathrm{O_2}}=k^{\mathrm{M}}_{\mathrm{V-D},b}n_{\mathrm{O}}n_{\mathrm{O}}n_{\mathrm{M}}-k^{\mathrm{M}}_{\mathrm{V-D},f}n_{\mathrm{O_2}}n_{\mathrm{M}}, \tag{2}$$

$$\omega_{\mathrm{O}}=-\omega_{\mathrm{O_2}}, \tag{3}$$

where N_{Av} is the Avogadro constant, M_s is the species molecular mass, n_s is the species number density, and $k_{\mathrm{V-D},f}$ and $k_{\mathrm{V-D},b}$ are the global dissociation and recombination rate coefficients, respectively, with their superscripts (M) representing the third particle. The global rate coefficients can be evaluated by

$$k^{\mathrm{M}}_{\mathrm{V-D},f}=Zk^{\mathrm{M}}_{\mathrm{V-D},f,\mathrm{eq}},\quad k^{\mathrm{M}}_{\mathrm{V-D},b}=\frac{k^{\mathrm{M}}_{\mathrm{V-D},f,\mathrm{eq}}}{K_{\mathrm{eq}}}, \tag{4}$$

where Z is the nonequilibrium factor, $k_{\mathrm{V-D},f,\mathrm{eq}}$ is the global dissociation rate coefficient at equilibrium, and K_{eq} is the equilibrium constant.

ω_{v} can be further decomposed into two parts as

$$\omega_{\mathrm{v}}=\omega_{\mathrm{V-T}}+\omega_{\mathrm{V-D}}, \tag{5}$$

where $\omega_{\mathrm{V-T}}$ represents the energy transfer between the vibrational and translational modes, and $\omega_{\mathrm{V-D}}$ represents the added or removed vibrational energy induced by recombination and dissociation.

This paper adopts Park's chemical reaction model [22] to calculate the equilibrium rate coefficients. $\omega_{\mathrm{V-T}}$ is modeled using the Landau-Teller model [1], in which the vibrational relaxation times are calculated with the Millikan-White expression [23]. For O_2-O_2 and O_2-O interactions, the original Millikan-White parameters were adjusted by Park [24] based on experimental data. Park's correction [22] is introduced to avoid underprediction of the relaxation times at high temperatures. The Marrone-Treanor model [4], also called the coupled vibration-dissociation-vibration (CVDV) model, is used to account for the vibration-dissociation coupling effects, which assumes that the dissociation probabilities scale exponentially with the vibrational levels. The corresponding Z can be expressed by

$$Z=\frac{Q_{\mathrm{v}}(T_{\mathrm{tr}})Q_{\mathrm{v}}(T_F)}{Q_{\mathrm{v}}(T_{\mathrm{v}})Q_{\mathrm{v}}(-U)}, \tag{6}$$

where Q_{v} is the vibrational partition function, U is an adjustable parameter in kelvins, and T_F is defined by

$$\frac{1}{T_F}=\frac{1}{T_{\mathrm{v}}}-\frac{1}{T_{\mathrm{tr}}}-\frac{1}{U}. \tag{7}$$

$\omega_{\mathrm{V-D}}$ can be obtained by

$$\omega_{\mathrm{V-D}}=\omega_b E(-U)-\omega_f E(T_F). \tag{8}$$

In this expression, ω_f and ω_b are the forward and backward mass production rates of O_2, and the weighted average vibrational energy is evaluated by

$$E(T)=\frac{R\theta_{\mathrm{v}}}{\exp(\theta_{\mathrm{v}}/T)-1}-\frac{R\theta_{\mathrm{d}}}{\exp(\theta_{\mathrm{d}}/T)-1}, \tag{9}$$

where R, θ_v, and θ_d are the gas constant, the characteristic vibrational temperature, and the characteristic dissociation temperature of O_2, respectively. Based on the comparison with state-specific data obtained using the forced harmonic oscillator (FHO) model and the quasi-classical trajectory (QCT) method, the semi-empirical parameter U is set to $\theta_d/3$ as reported by Hao *et al.* [25].

B. Maximum entropy models

The ME principle [15] proposes that molecular collisions tend to produce post-collision distributions that maximize entropy. It has been applied to interpret the state-specific cross sections of, and to build reduced models of, vibrational relaxation and dissociation, assuming appropriate prior distributions and surprisal functions. The idea was recently generalized in Refs. [10–14] and blended with modern numerical techniques by introducing group and reconstruction concepts. Specifically, the vibrational state population density can be expressed as

$$\ln n_{O_2(i)} = \alpha + \beta\varepsilon_i + \gamma\varepsilon_i^2 + \cdots, \tag{10}$$

subject to the macroscopic constraints

$$\sum_i n_{O_2(i)} = n_{O_2}, \quad \sum_i n_{O_2(i)}\varepsilon_i = e_v, \quad \sum_i n_{O_2(i)}\varepsilon_i^2 = f_v, \tag{11}$$

However, it is important to note that including the nonlinear terms seems to be a purely numerical treatment without experimental justification.

In this work, two generalized ME models are established for oxygen, representing the logarithms of distribution functions by linear and quadratic functions, respectively. The entire vibrational energy ladder is treated as a single group.

1. Maximum entropy linear model

In the ME linear model, the vibrational state population distribution is given by

$$\ln n_{O_2(i)} = \alpha + \beta\varepsilon_i, \tag{12}$$

where α and β are the Lagrange multipliers, and ε_i is the vibrational energy of the ith vibrational quantum state. Evidently, the ME linear model acknowledges that the vibrational level distribution can be described by the Boltzmann distribution. The vibrational temperature T_v is related to β via

$$\beta = -\frac{1}{k_B T_v}, \tag{13}$$

where k_B represents the Boltzmann constant. The governing equations are the same as Eq. (1). To evaluate ω_s and ω_v, the ME linear model abandons the relatively rigorous assumptions adopted by the conventional 2-T model but accounts for the elementary kinetics instead. The ME linear model can therefore be regarded as the upper performance limit of a 2-T model.

In this paper, vibration-vibration-translation (V-V-T) bound-bound transitions induced by O_2 impacts, vibration-translation (V-T) bound-bound transitions induced by O impacts, and vibration-dissociation (V-D) bound-free transitions are considered and can be expressed as follows:

$$O_2(i) + O_2(j) \leftrightarrow O_2(l) + O_2(m), \tag{14}$$

$$O_2(i) + O \leftrightarrow O_2(j) + O, \tag{15}$$

$$O_2(i) + M \leftrightarrow O + O + M, \tag{16}$$

where i, j, l, and m represent the vibrational quantum numbers of O_2.

$\omega_{\underline{s}}$ for O_2 and O can also be evaluated via Eqs. (2) and (3). The global dissociation and recombination rate coefficients are obtained by

$$k^{\mathrm{M}}_{\mathrm{V-D},f} = \sum_i k^{\mathrm{M}}_{\mathrm{V-D}}(i \to c)\frac{n_{\mathrm{O}_2(i)}}{n_{\mathrm{O}_2}}, \tag{17}$$

$$k^{\mathrm{M}}_{\mathrm{V-D},b} = \sum_i k^{\mathrm{M}}_{\mathrm{V-D}}(c \to i), \tag{18}$$

where $k_{\mathrm{V-D}}(i \to c)$ and $k_{\mathrm{V-D}}(c \to i)$ are the forward and backward rate coefficients of the V–D transitions, respectively. Furthermore, $\omega_{\mathrm{V-T}}$ can be obtained by

$$\begin{aligned}\omega_{\mathrm{V-T}} = &\sum_i \varepsilon_i \sum_j \sum_l \sum_m k_{\mathrm{V-V-T}}(l, m \to i, j) n_{\mathrm{O}_2(l)} n_{\mathrm{O}_2(m)} \\ &- \sum_i \varepsilon_i \sum_j \sum_l \sum_m k_{\mathrm{V-V-T}}(i, j \to l, m) n_{\mathrm{O}_2(i)} n_{\mathrm{O}_2(j)} \\ &+ \sum_i \varepsilon_i \sum_j \left[k_{\mathrm{V-T}}(j \to i) n_{\mathrm{O}_2(j)} n_{\mathrm{O}} - k_{\mathrm{V-T}}(i \to j) n_{\mathrm{O}_2(i)} n_{\mathrm{O}}\right],\end{aligned} \tag{19}$$

where $k_{\mathrm{V-V-T}}(i, j \to l, m)$ and $k_{\mathrm{V-T}}(i \to j)$ are the forward rate coefficients of the V-V-T and V-T transitions, respectively. $\omega_{\mathrm{V-D}}$ can be written as

$$\omega_{\mathrm{V-D}} = \omega_b E_b - \omega_f E_f, \tag{20}$$

where the terms that represent the forward and backward weighted average vibrational energy, E_f and E_b, are given by

$$E_f = \sum_i \varepsilon_i \frac{k^{\mathrm{M}}_{\mathrm{V-D}}(i \to c)}{k^{\mathrm{M}}_{\mathrm{V-D},f}} \frac{n_{\mathrm{O}_2(i)}}{n_{\mathrm{O}_2}}, \tag{21}$$

$$E_b = \sum_i \varepsilon_i \frac{k^{\mathrm{M}}_{\mathrm{V-D}}(c \to i)}{k^{\mathrm{M}}_{\mathrm{V-D},b}}. \tag{22}$$

In the ME linear model, the 47 vibrational levels given by Andrienko and Boyd [26] are considered for molecular oxygen in the ground electronic state. The O_2-O_2 V-V-T transition rate coefficients are generated using the FHO model [27,28]. According to the state-specific results of Hao *et al.* [7], multi-quantum V-V-T transitions with jumps larger than 5 are neglected to reduce the computational burden. The O_2-O_2 V-D rate coefficients are taken from the FHO analysis of Lino da Silva *et al.* [29], and the O_2-O V-T and V-D rate coefficients are obtained from the QCT calculations of Andrienko and Boyd [30,31]. Note that all jumps are considered for the V-T and V-D transitions. The rate coefficients of the forward and backward processes can be correlated using the principle of detailed balance.

2. Maximum entropy quadratic model

In the ME quadratic model, the vibrational state population distribution is given by

$$\ln n_{\mathrm{O}_2(i)} = \alpha + \beta\varepsilon_i + \gamma\varepsilon_i^2, \tag{23}$$

where γ is the third Lagrange multiplier. In contrast to the ME linear model, the ME quadratic model assumes that the logarithm of the distribution function is quadratic. The vibrational temperature T_{v} controlling the slope of the distribution at lower vibrational levels can be defined by

$$\beta = -\frac{1}{k_B T_{\mathrm{v}}}. \tag{24}$$

In addition, a dissociation temperature T_d that describes the slope at higher levels can be defined as

$$\gamma = \frac{1}{2\varepsilon_\mathrm{d}}\left[\frac{1}{k_B T_\mathrm{v}} - \frac{1}{k_B T_\mathrm{d}}\right], \tag{25}$$

where ε_d is the dissociation energy. If the vibrational energy e_v is regarded as the first-order moment in terms of the vibrational energy level populations, the second-order moment f_v can be defined as

$$f_\mathrm{v} = \frac{N_\mathrm{Av}}{M_{\mathrm{O}_2}} \sum_i \varepsilon_i^2 \frac{n_{\mathrm{O}_2(i)}}{n_{\mathrm{O}_2}}. \tag{26}$$

To close the governing equations, an additional conservation equation of f_v is required and can be expressed as

$$\frac{\partial}{\partial x}(\rho u f_\mathrm{v}) = \omega'_\mathrm{v}. \tag{27}$$

After the upgrade of e_v and f_v, T_v and T_d can be evaluated using Newton's iteration, and thus the vibrational populations are obtained.

In this model, ω_s and ω_v are calculated in the same way as in the ME linear model. Similar to ω_v, ω'_v is also composed of two parts, $\omega'_{\mathrm{V-T}}$ and $\omega'_{\mathrm{V-D}}$, the expression of which can be readily obtained by replacing ε_i in Eqs. (19), (21), and (22) with ε_i^2 as follows:

$$\begin{aligned}\omega'_{\mathrm{V-T}} = &\sum_i \varepsilon_i^2 \sum_j \sum_l \sum_m k_{\mathrm{V-V-T}}(l, m \to i, j) n_{\mathrm{O}_2(l)} n_{\mathrm{O}_2(m)} \\ &- \sum_i \varepsilon_i^2 \sum_j \sum_l \sum_m k_{\mathrm{V-V-T}}(i, j \to l, m) n_{\mathrm{O}_2(i)} n_{\mathrm{O}_2(j)} \\ &+ \sum_i \varepsilon_i^2 \sum_j \left[k_{\mathrm{V-T}}(j \to i) n_{\mathrm{O}_2(j)} n_\mathrm{O} - k_{\mathrm{V-T}}(i \to j) n_{\mathrm{O}_2(i)} n_\mathrm{O}\right],\end{aligned} \tag{28}$$

$$\omega'_{\mathrm{V-D}} = \omega_b \sum_i \varepsilon_i^2 \frac{k^\mathrm{M}_{\mathrm{V-D}}(c \to i)}{k^\mathrm{M}_{\mathrm{V-D},b}} - \omega_f \sum_i \varepsilon_i^2 \frac{k^\mathrm{M}_{\mathrm{V-D}}(i \to c)}{k^\mathrm{M}_{\mathrm{V-D},f}} \frac{n_{\mathrm{O}_2(i)}}{n_{\mathrm{O}_2}}. \tag{29}$$

The vibrational energy ladder and the transition rate coefficients are the same as those incorporated in the ME linear model.

C. State-specific method

The state-specific method traces the temporal and spatial variation of each vibrational energy state and thus significantly increases the number of equations to be solved; however, it no longer makes assumptions on the formulation of the vibrational level distribution. The state-specific method can be regarded as the most rigorous approach to describe vibrational excitation and dissociation and thus a reliable reference to evaluate reduced models. The corresponding governing equations are given by

$$\begin{aligned}\frac{\partial}{\partial x}[\rho_{\mathrm{O}_2(i)} u] &= \omega_{\mathrm{O}_2(i)}, \quad i = 0, 1, \ldots, 47, \\ \frac{\partial}{\partial x}(\rho_\mathrm{O} u) &= \omega_\mathrm{O}, \\ \frac{\partial}{\partial x}(\rho u^2 + p) &= 0, \\ \frac{\partial}{\partial x}\left[\rho u\left(h + \frac{1}{2}u^2\right)\right] &= 0.\end{aligned} \tag{30}$$

TABLE I. Flow conditions for shock tube experiments [32].

Case no.	V_s (m/s)	p_1 (Torr)	T_1 (K)
1	3070	2.0	295
2	3950	1.0	295
3	4440	0.8	295

The mass production rate of O_2 at the ith vibrational level can be readily calculated based on the kinetic rates as

$$\begin{aligned}\frac{N_{\mathrm{Av}}}{M_{\mathrm{O}_2}}\omega_{\mathrm{O}_2(i)} = &\sum_j\sum_l\sum_m k_{\mathrm{V-V-T}}(l,m\rightarrow i,j)n_{\mathrm{O}_2(l)}n_{\mathrm{O}_2(m)}\\ &-\sum_j\sum_l\sum_m k_{\mathrm{V-V-T}}(i,j\rightarrow l,m)n_{\mathrm{O}_2(i)}n_{\mathrm{O}_2(j)}\\ &+\sum_j\left[k_{\mathrm{V-T}}(j\rightarrow i)n_{\mathrm{O}_2(j)}n_{\mathrm{O}}-k_{\mathrm{V-T}}(i\rightarrow j)n_{\mathrm{O}_2(i)}n_{\mathrm{O}}\right]\\ &+k^{\mathrm{M}}_{\mathrm{V-D}}(c\rightarrow i)n^2_{\mathrm{O}}n_{\mathrm{M}}-k^{\mathrm{M}}_{\mathrm{V-D}}(i\rightarrow c)n_{\mathrm{O}_2(i)}n_{\mathrm{M}}.\end{aligned}\tag{31}$$

One can easily identify the contributions of different types of transitions in Eq. (31). The vibrational energy ladder and the transition rate coefficients are the same as those in the ME linear model. For comparison with the results of the other models and experimental data, a vibrational temperature T_{v} is defined as

$$T_{\mathrm{v}}=\frac{\varepsilon_1-\varepsilon_0}{k_B\ln[n_{\mathrm{O}_2(1)}/n_{\mathrm{O}_2(0)}]}.\tag{32}$$

Notably, this T_{v} is defined based on the first-level vibrational energy.

III. RESULTS

A. Comparison with experiments

In this section, thermochemical nonequilibrium flows of oxygen behind normal shocks are investigated under conditions corresponding to a set of experiments conducted by Ibraguimova *et al.* [32]. The focus will be on comparing the predictions of the 2-T and ME models with the state-specific results and the experimental data.

The test cases represent a relevant range of conditions that might be encountered during hypersonic flight. The recent experiments by Ibraguimova *et al.* [32] determined the vibrational temperature profiles of oxygen behind the shock fronts in a shock tube, with the translational temperature immediately across the shock ranging from 4000 to 10 800 K. Herein, the stationary test gas in the low-pressure chamber is pure oxygen. Table I summarizes the three cases considered for the present simulations, where V_s represents the velocity of the shock wave, and p_1 and T_1 are the pressure and temperature ahead of the shock front, respectively. The post-shock distributions of the translational-rotational temperature and the concentration of atomic oxygen were also calculated by solving the gas dynamics equations at the measured vibrational temperatures. With the increase of the post-shock translational temperature, the process of vibrational excitation and dissociation becomes increasingly intense from cases 1 to 3.

In the shock reference frame, the governing equations given in Sec. II can be solved using the space-marching method. The initial condition is derived from the Rankine-Hugoniot relations assuming frozen vibrational mode and chemical composition. The explicit fourth-order Runge-Kutta scheme is used for numerical integration.

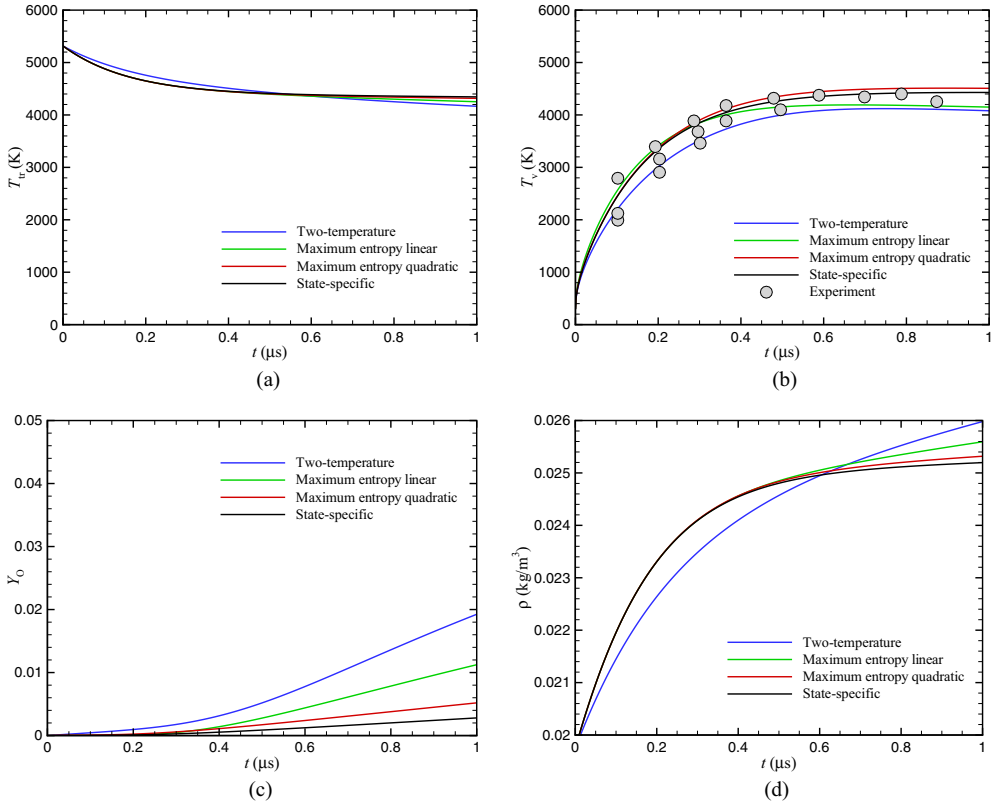

FIG. 1. Post-shock profiles for case 1 (a) Translationalrotational temperature, (b) Vibrational temperature, (c) Mass fraction of O, and (d) Mixture density.

Figures 1–3 show the post-shock profiles of translational-rotational temperature, vibrational temperature, mass fraction of O, and mixture density predicted using different modeling approaches for cases 1–3, respectively. Also shown in the figures are the experimental data, if available. Note that time is related to the distance from the shock via $t = x/V_s$.

For case 1, every model yields similar temperature distributions and agrees well with the high-fidelity state-specific method and the experiments. In fact, case 1 corresponds to a relatively moderate condition in which T_{tr} immediately across the shock is equal to 5300 K. As a result, there is only a small amount of O, as seen in Fig. 1(c). At $t = 1\,\mu$s, the mass fractions of O predicted by the models are less than 2%. Under this condition, the vibration-dissociation coupling effects are weak and the flow is dominated by vibrational relaxation due to O_2-O_2 interactions, which is well described by the Landau-Teller model. In addition, because the non-Boltzmann effects are insignificant, only slight differences are observed between the results from the two ME models.

For case 2, the post-shock T_{tr} reaches 8620 K, leading to much greater dissociation. As seen in Fig. 2, the 2-T model fails to reproduce the state-specific results and the experimental data, presenting a much lower T_{tr} and larger degree of dissociation. The mixture density is inversely proportional to T_{tr} and is thus significantly overestimated. The ME linear model yields more accurate predictions than the conventional 2-T model. The differences can be attributed to the modeling errors in the 2-T model, especially regarding the vibration-dissociation coupling. However, room remains for improvement in the ME linear model.

Notably, when the non-Boltzmann effects are accounted for in the ME quadratic model, good agreement with the state-specific results is obtained in terms of the translational-rotational

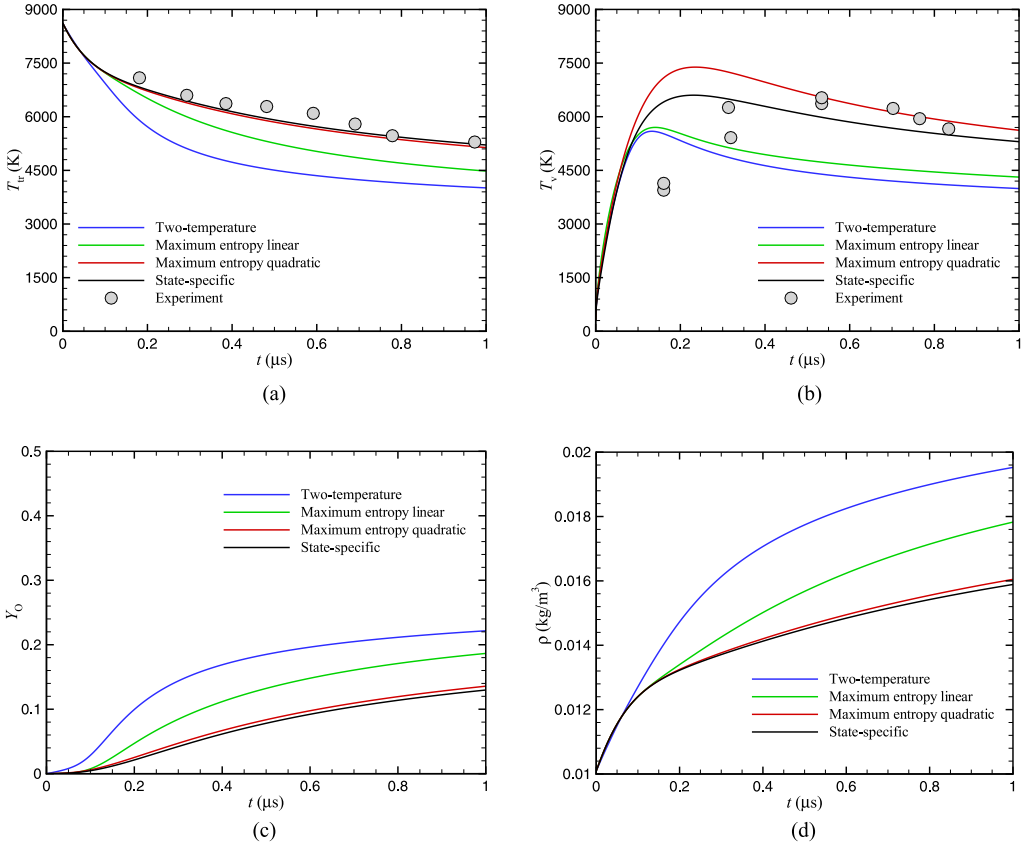

FIG. 2. Post-shock profiles for case 2 (a) Translationalrotational temperature, (b) Vibrational temperature, (c) Mass fraction of O, and (c) Mass fraction of O.

temperature, mass fraction of O, and mixture density. The ME quadratic behaviors also closely follow the shock tube data. It is well known that higher vibrational levels are significantly overpopulated as a result of vibrational excitation during the incubation time (i.e., $t < 0.1\ \mu$s). Afterward, dissociation dominates the nonequilibrium process, leading to an underpopulation of the higher levels. The large difference between the two ME models indicates that such non-Boltzmann distribution effects play an important role under conditions similar to case 2. Figure 2(b) shows that the vibrational temperature profile predicted by the ME quadratic model deviates from the state-specific result. This deviation is reasonable because of the different definitions of T_v in these two approaches. In fact, the T_v shown in the figure for the state-specific method is defined using the first level, whereas in the ME quadratic model it represents the overall behavior of the lower levels. Separating the vibrational levels into more groups would reduce the difference; however, the present results suggest that the use of one group is enough to capture the macroscopic flowfield quantities under the considered conditions.

Case 3 corresponds to the highest degree of nonequilibrium among the three cases, with T_{tr} of 10 820 K immediately across the shock. Similar to case 2, the 2-T and ME linear models fail to accurately describe the trends of the state-specific results and the experimental data. In contrast, the ME quadratic model makes an accurate prediction. Note that the experimental data of the species mass fraction are available for case 3, as shown in Fig. 3(c). The results from the ME quadratic model and the state-specific method almost perfectly overlap, and generally match the measurements. However, some discrepancies appear in the vicinity of $t = 0.2\ \mu$s, which can be attributed to the modeling errors of vibrational kinetic rates and to the measurement uncertainties.

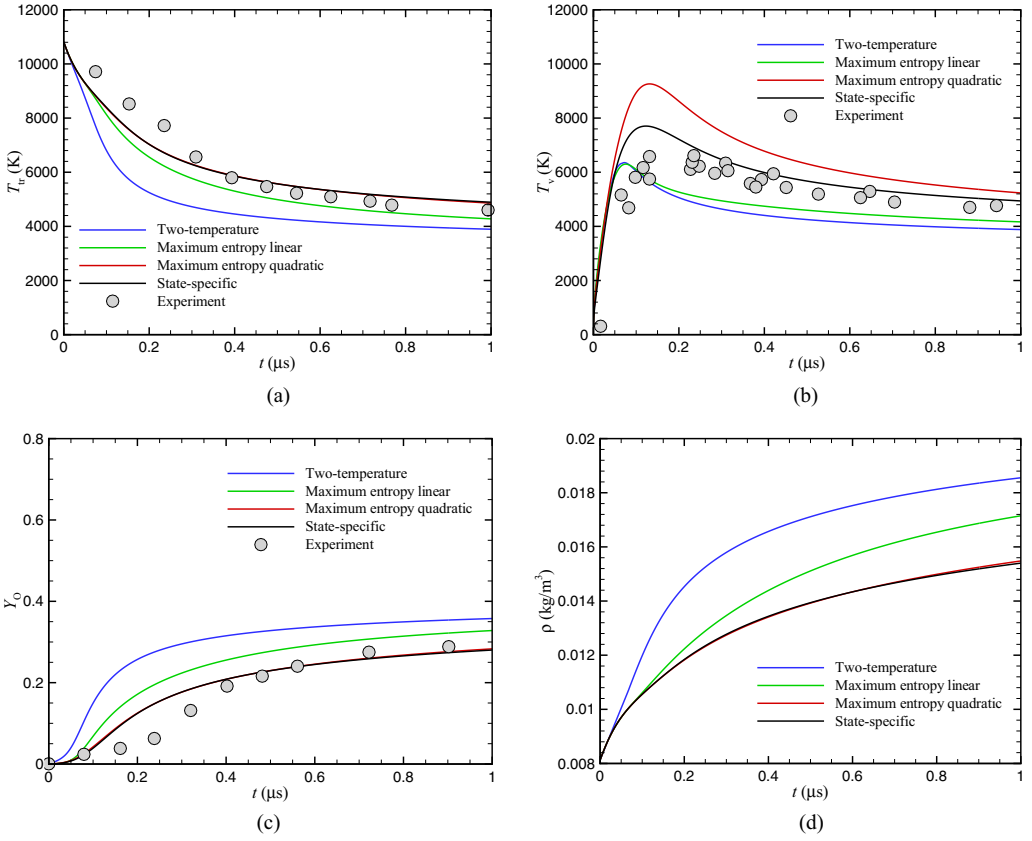

FIG. 3. Post-shock profiles for case 3 (a) Translationalrotational temperature, (b) Vibrational temperature, (c) Mass fraction of O, and (d) Mixture density.

In general, the ME quadratic model accurately captures the vibrational excitation and dissociation, especially in terms of the post-shock translational-rotational temperature, species mass fraction, and mixture density. However, it is important to note some disagreements between the vibrational temperatures predicted by the ME quadratic model and the state-specific method for all three cases. These disagreements result from representing the entire vibrational energy level populations using a quadratic function, which inevitably introduces errors. The errors could be compensated by separating the vibrational levels into several groups [12]. Nevertheless, the results of this study verify that the use of only one group is adequate for accurate prediction of the flow quantities. This argument is further supported by the post-shock profiles of specific vibrational energy predicted by the various models for cases 1–3 as shown in Fig. 4. Although the vibrational temperature is not captured correctly, the vibrational energy is accurately predicted, which indicates that the energy allocation among the internal energy modes is well described by the ME quadratic model.

The good performance of the ME quadratic model highlights the role of non-Boltzmann effects in vibrational nonequilibrium modeling. Another approach to consider the non-Boltzmann distributions is to divide the vibrational energy ladder into larger numbers of groups in the ME linear model. Figure 5 shows the post-shock distributions of temperature and species mass fraction predicted using the ME linear model with different internal groupings for case 3, and compares the results with those obtained using the ME quadratic model and the state-specific method. Note that the vibrational energy ladder is divided uniformly for each grouping. As seen in the figure, the

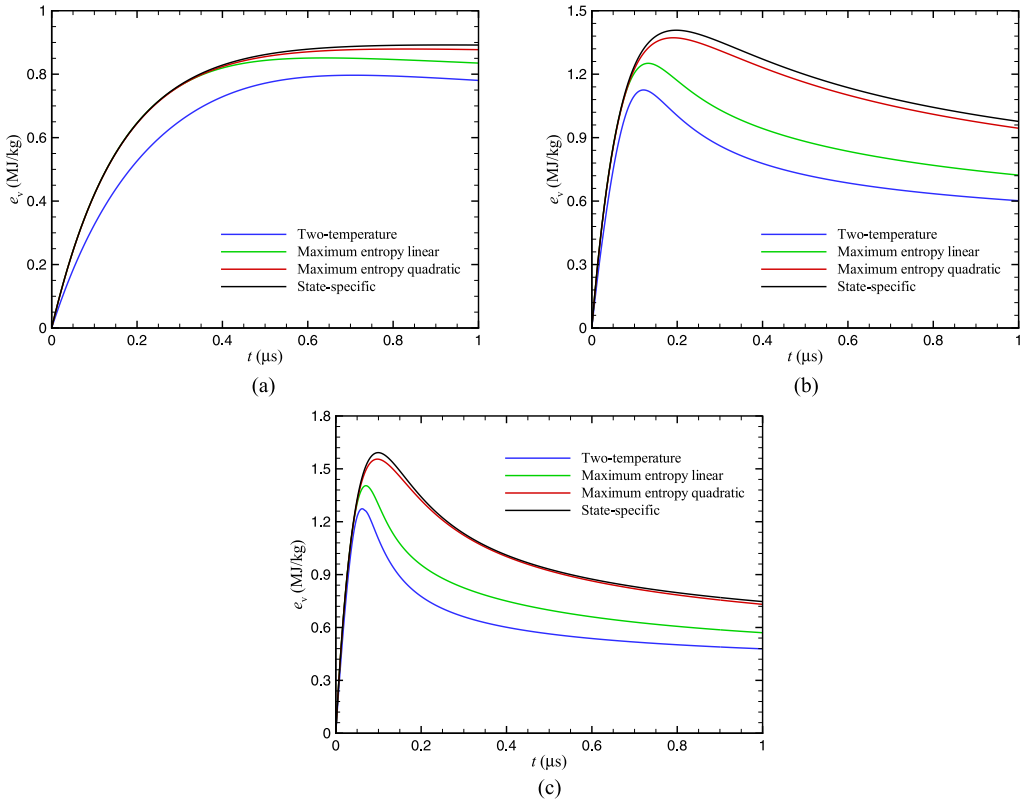

FIG. 4. Specific vibrational energy profiles for different cases (a) Case 1, (b) Case 2, and (c) Case 3.

predictive accuracy of the ME linear model is significantly improved by including more groups. However, the number of equations to be solved increases with the number of internal groups, which is detrimental to the model's application for large-scale simulations.

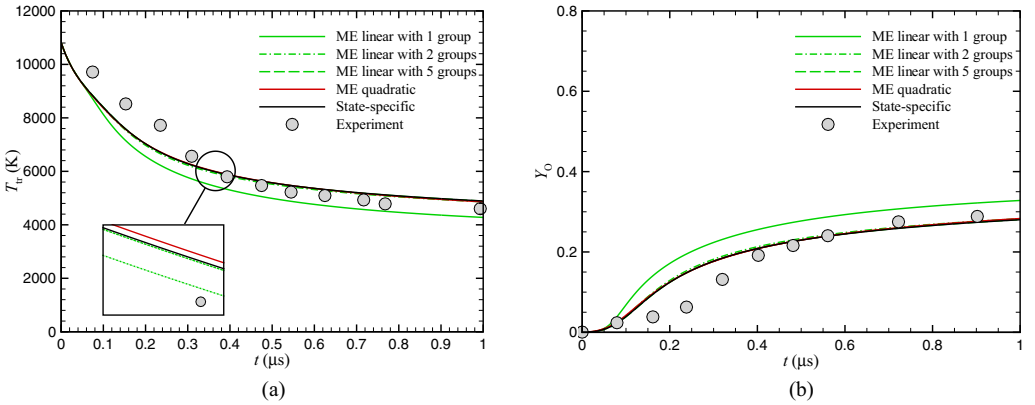

FIG. 5. Post-shock profiles for case 3 showing the effects of a larger number of internal groups (a) Translationalrotational temperature, and (b) Mass fraction of O.

TABLE II. CPU time per 1000 iterations for different models.

Model	2-T	ME linear	ME quadratic	Modified ME quadratic	State specific
CPU time (s)	0.0624	240.6471	236.7627	0.8892	225.8738

B. A modified model for CFD applications

Despite treating the entire vibrational ladder as a single group, the ME quadratic model is still computationally expensive, hindering its CFD applications. Note that 48^4 rate coefficients would be required to construct a complete data set for the O_2-O_2 V-V-T transitions at a given T_{tr}. By invoking the principle of detailed balance and neglecting multi-quantum jumps larger than 5, the number of V-V-T rate coefficients is significantly reduced; however, the use of such a large-scale database in practical calculations still causes high memory and CPU usage.

Table II presents the CPU times consumed by different models for 1000 iterations of the post-shock calculations. The 2-T model is the most computationally efficient, with a CPU time less than 0.03% of that for the state-specific method. Interestingly, the ME models consume even more CPU time than the high-fidelity approach. This reflects the use of Newton's iteration in the ME models to determine T_v and T_d, which increases the computational cost despite the reduced number of equations to be solved.

In the 2-T interpretation, vibrational excitation and dissociation are modeled separately. The relaxation of the vibrational energy is described by the Landau-Teller theory, which assumes that the transitions occur only between the neighboring states and that the transition rates are proportional to the quantum number [22]. These assumptions are invalid under strongly nonequilibrium conditions; however, the general behavior of vibrational relaxation can be largely captured using appropriate relaxation times [33]. Therefore, it is proposed in this paper to simplify the ME quadratic model into a computationally affordable form by representing the evolutions of both e_v and f_v in the Landau-Teller expression.

1. Heat bath calculations

Heat bath calculations are the usual approach to study vibrational relaxation while excluding the process of dissociation. Various state-specific calculations [26,31,33,34] in O_2-O mixtures under heat bath conditions have been conducted. The resulting relaxation times are in good agreement with existing experimental data, presenting a different temperature dependence from the Millikan-White expression. This study has no intention of reproducing the vibrational relaxation times but focuses on the behavior of the second-order moment f_v.

Two heat bath conditions are considered in this paper, similar to those reported by Andrienko and Boyd [31]. The initial number density is set to 10^{18} cm^{-1}. All particles are assumed to be O_2 when studying the O_2-O_2 system, whereas the mole concentration of O is set to 0.99 for O_2-O interactions. The initial population of the vibrational states is assumed to be in the Boltzmann distribution at 100 K. Furthermore, the environmental temperatures range from 1000 to 10 000 K and remain unchanged during the calculation.

The heat bath calculations are performed using the state-specific method. The corresponding equations are similar to Eq. (28), except that the convective term is replaced by the temporal term of conserved variables. Again, the explicit fourth-order Runge-Kutta scheme is adopted for numerical integration.

If the nonequilibrium process is assumed to follow the Landau-Teller equation, the temporal evolutions of e_v and f_v can be expressed as

$$\frac{de_v(t)}{dt} = \frac{e_{v,eq} - e_v(t)}{\tau_e}, \tag{33}$$

$$\frac{df_v(t)}{dt} = \frac{f_{v,eq} - f_v(t)}{\tau_f}. \tag{34}$$

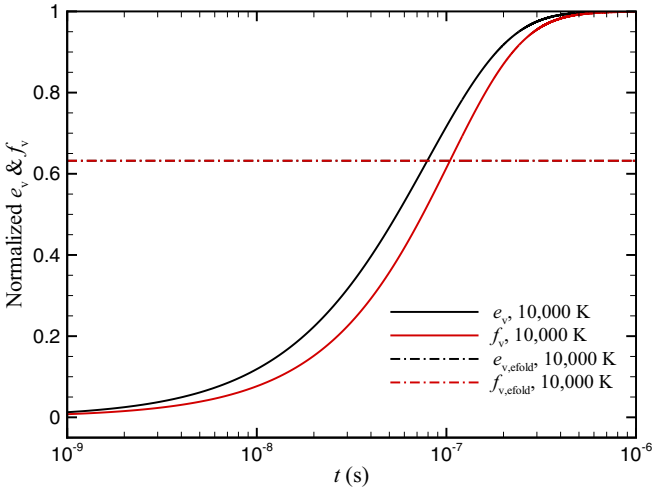

FIG. 6. Evolutions of e_v and f_v for O_2-O interactions at heat bath temperature of 10 000 K.

In these expressions, $e_{v,eq}$ and $f_{v,eq}$ represent the equilibrium values that correspond to the environmental temperature, and the relaxation times τ_e and τ_f can be obtained using the e-folding method. The corresponding e-folding values are defined by

$$e_{v,efold} = \frac{1}{e} e_v(0) + \left(1 - \frac{1}{e}\right) e_{v,eq}, \tag{35}$$

$$f_{v,efold} = \frac{1}{e} f_v(0) + \left(1 - \frac{1}{e}\right) f_{v,eq}. \tag{36}$$

Figure 6 shows the evolutions of e_v and f_v obtained from the state-specific calculations for O_2-O collisions at a heat bath temperature of 10 000 K. Note that e_v and f_v have been normalized by the respective equilibrium values. Because e_v and f_v at the initial state are negligible compared with their final values, the dash-dotted lines standing for normalized $e_{v,efold}$ and $f_{v,efold}$ almost perfectly overlap. The relaxation times can be readily determined from this figure. Similar results can be derived by the e-folding method for O_2-O_2 collisions.

TABLE III. Vibrational relaxation curve-fitting coefficients for O_2-O_2 interactions.

Coefficients	$p\tau_e$	$p\tau_f$
c_{-3}	8.9666	11.1073
c_{-2}	−28.3842	−36.1095
c_{-1}	49.9322	65.4861
c_0	−34.5109	−41.7713
c_1	−4.2005	−6.9750
c_2	2.7543×10^{-1}	5.0196×10^{-1}
c_3	-1.1132×10^{-2}	-2.2584×10^{-2}
c_4	1.9522×10^{-4}	4.3745×10^{-4}
c_5	16.2030	25.0828

TABLE IV. Vibrational relaxation curve-fitting coefficients for O_2-O interactions.

	a	b	C	d	e
$p\tau_e$	9.7511×10^{-4}	-2.1780×10^{-2}	1.3094×10^{-1}	8.8263×10^{-1}	1.0567
$p\tau_f$	1.3222×10^{-3}	-2.8042×10^{-2}	1.4436×10^{-1}	1.4014	7.4968×10^{-1}

The resulting vibrational relaxation times for O_2-O_2 interactions can be curve-fitted by a polynomial function as

$$p\tau = \exp\left[\sum_{k=-3}^{4} c_k \left(\frac{T_{\mathrm{tr}}}{1000}\right)^k + c_5 \log\left(\frac{T_{\mathrm{tr}}}{1000}\right)\right]. \tag{37}$$

As suggested by Andrienko and Boyd [26], the vibrational times for O_2-O interactions can be well represented by the following function:

$$p\tau = 10^{-8}\left[a\left(\frac{T}{1000}\right)^4 + b\left(\frac{T}{1000}\right)^3 + c\left(\frac{T}{1000}\right)^2 + d\left(\frac{T}{1000}\right) + e\right]. \tag{38}$$

In the above equations, p is the pressure in atmospheres and the curve-fitting coefficients are given in Tables III and IV.

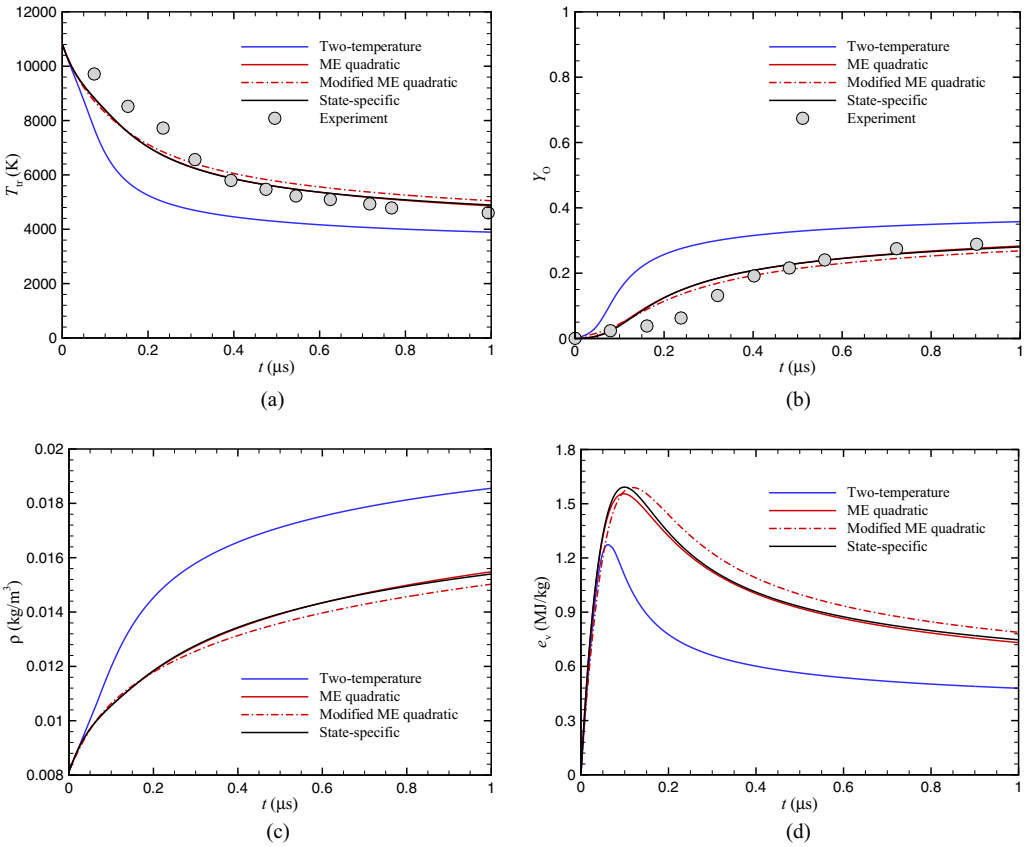

FIG. 7. Post-shock profiles for case 3 (a) Translationalrotational temperature, (b) Mass fraction of O, (c) Mixture density, and (d) Specific vibrational energy.

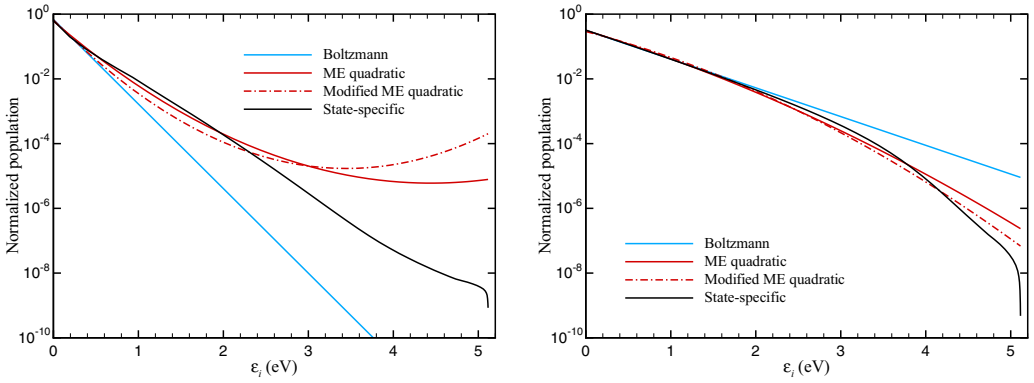

FIG. 8. Vibrational energy level populations for case 3 (a) $t = 0.01\ \mu$s, (b) $t = 0.5\ \mu$s.

2. Post-shock flows

A modified ME quadratic model can be established by acknowledging that the relaxation of e_v and f_v can be described by the Landau-Teller model. When applied to post-shock flows, the governing equations are similar to those given in Sec. II B 1. The only modification is to reformulate the vibration-translation terms ω_{V-T} and ω'_{V-T} using the Landau-Teller expression with the relaxation times given in Sec. III B 1.

In this section, the post-shock flow conditions corresponding to the experiments of Ibraguimova *et al.* [32] are revisited to validate the established model. Only case 3 with the strongest nonequilibrium is considered here. Figure 7 shows the post-shock profiles of translational-rotational temperature, mass fraction of O, mixture density, and specific vibrational energy for case 3. For clarity, the results from the ME linear model are excluded. Note that the vibrational temperature profiles are not presented, because capturing the vibrational energy is more relevant than reproducing the experimental data of T_v. The modified model shows some differences from the results of the ME quadratic model. Nevertheless, the modified model generally captures the state-specific and experimental behaviors and achieves a significant improvement over the 2-T model. Most importantly, the CPU time is reduced to 0.8892 s per 1000 iterations, which makes it feasible to incorporate this model in CFD solvers.

To further demonstrate the effect of the proposed model on the process of vibrational excitation and dissociation, the normalized populations of vibrational energy levels predicted using different models at $t = 0.01$ and $0.5\ \mu$s for case 3 are compared in Fig. 8. Also shown in the figure are the Boltzmann distributions calculated under local conditions. Note that the Boltzmann distributions are exactly straight lines in logarithmic coordinates. It is seen that the proposed model with the Landau-Teller formulation for vibrational excitation can reproduce the distributions predicted by the original ME quadratic model, and both can capture the state-specific behaviors qualitatively. Compared with the Boltzmann distributions, the high-lying levels are overpopulated due to vibrational excitation at $t = 0.01\ \mu$s, whereas an obvious underpopulation of the upper energy states occurs at $t = 0.5\ \mu$s due to preferential dissociation. Increasing the number of groups would improve the accuracy of the original and modified ME quadratic models; however, this study suggests that the use of a single group is adequate given that macroscopic quantities are of more concern for CFD applications.

IV. CONCLUSIONS

Various models of vibrational excitation and dissociation with a range of fidelity were used to simulate nonequilibrium flows behind a normal shock under conditions corresponding to recent shock tube experiments. The results were compared with the experimental data.

A conventional 2-T model, two improved models based on the ME principle, and the state-specific method were considered. The 2-T calculations used the Landau-Teller model and the CVDV model to describe vibrational relaxation and vibration-dissociation coupling effects. The ME linear and quadratic models were established on the assumption that the vibrational energy levels can be interpreted by linear and quadratic functions. Finally, the state-specific method traced the temporal and spatial variation of each vibrational energy state and thus had the highest fidelity.

The post-shock simulations demonstrated that the 2-T results significantly deviated from the experiments, especially under conditions of strong nonequilibrium. The ME linear model showed some improvement but still lacked sufficient accuracy. By contrast, the ME quadratic model accurately captured the state-specific and experimental behaviors in terms of translational-rotational temperature, mass fraction of atomic O, mixture density, and specific vibrational energy. However, this model was still very computationally expensive.

To reduce the computational cost, it was proposed that the relaxation of the first-order and second-order moments could be described by the Landau-Teller formulation. The corresponding relaxation times were determined from state-specific heat bath calculations. The post-shock flows were revisited using the modified ME quadratic model. The new model maintained sufficient prediction accuracy while reducing the CPU time significantly, indicating its feasibility to be further incorporated in CFD solvers.

ACKNOWLEDGMENT

The authors would like to thank the Hong Kong Research Grants Council (Grant No. 15215116) for financial support.

[1] W. G. Vincenti and C. H. Kruger, *Introduction to Physical Gas Dynamics* (Krieger, Malabar, FL, 1965).

[2] C. Park, Assessment of a two-temperature kinetic model for dissociating and weakly ionizing nitrogen, J. Thermophys. Heat Transfer **2**, 8 (1988).

[3] C. F. Hansen, Vibrational nonequilibrium effects on diatomic dissociation rates, AIAA J. **31**, 2047 (1993).

[4] P. V. Marrone and C. E. Treanor, Chemical relaxation with preferential dissociation from excited vibrational levels, Phys. Fluids **6**, 1215 (1963).

[5] P. Hammerling, J. Teare, and B. Kivel, Theory of radiation from luminous shock waves in nitrogen, Phys. Fluids **2**, 422 (1959).

[6] S. O. Macheret, A. A. Fridman, I. V. Adamovich, J. W. Rich, and C. E. Treanor, Mechanisms of nonequilibrium dissociation of diatomic molecules, in *6th Joint Thermophysics and Heat Transfer Conference Colorado Springs, CO, USA, 1994* (AIAA, Reston, VA, 2012).

[7] J. Hao, J. Wang, and C. Lee, State-specific simulation of oxygen vibrational excitation and dissociation behind a normal shock, Chem. Phys. Lett. **681**, 69 (2017).

[8] F. Bonelli, M. Tuttafesta, G. Colonna, L. Cutrone, and G. Pascazio, An MPI-CUDA approach for hypersonic flows with detailed state-to-state air kinetics using a GPU cluster, Comput. Phys. Commun. **219**, 178 (2017).

[9] I. D. Boyd and E. Josyula, Detailed analysis of vibrational nonequilibrium of molecular oxygen in shock-heated flow, Phys. Rev. Fluids **2**, 123401 (2017).

[10] Y. Liu, M. Panesi, A. Sahai, and M. Vinokur, General multi-group macroscopic modeling for thermo-chemical non-equilibrium gas mixtures, J. Chem. Phys. **142**, 134109 (2015).

[11] A. Munafò, Y. Liu, and M. Panesi, Modeling of dissociation and energy transfer in shock-heated nitrogen flows, Phys. Fluids **27**, 127101 (2015).

[12] M. S. Priyadarshini, Y. Liu, and M. Panesi, Advanced modeling of non-equilibrium flows using a maximum entropy quadratic formulation, *55th AIAA Aerospace Sciences Meeting, Grapevine, Texas, 2017* (AIAA, Reston, VA, 2017).

[13] R. L. Macdonald, R. L. Jaffe, D. W. Schwenke, and M. Panesi, Construction of a coarse-grain quasi-classical trajectory method. I. Theory and application to N_2-N_2 system, J. Chem. Phys. **148**, 054309 (2018).
[14] R. L. Macdonald, M. S. Grover, T. E. Schwartzentruber, and M. Panesi, Construction of a coarse-grain quasi-classical trajectory method. II. Comparison against the direct molecular simulation method, J. Chem. Phys. **148**, 054310 (2018).
[15] R. D. Levin and R. B. Bernstein, *Molecular Reaction Dynamics and Chemical Reactivity* (Oxford University Press, New York, 1987).
[16] S. Doraiswamy, J. D. Kelley, and G. V. Candler, Generalized chemistry—internal energy coupling model using prior recombination distribution, J. Thermophys. Heat Transfer **27**, 382(2013).
[17] M. A. Gallis and J. K. Harvey, Maximum entropy analysis of chemical reaction energy dependence, J. Thermophys. Heat Transfer **10**, 217 (1996).
[18] M. Kulakhmetov, M. Gallis, and A. Alexeenko, *Ab initio*-informed maximum entropy modeling of rovibrational relaxation and state-specific dissociation with application to the $O_2 + O$ system, J. Chem. Phys. **144**, 174302 (2016).
[19] D. A. Gonzales and P. L. Varghese, A simple model for state-specific diatomic dissociation, J. Phys. Chem. **97**, 7612 (1993).
[20] D. A. Gonzales and P. L. Varghese, Evaluation of simple rate expressions for vibration-dissociation coupling, J. Thermophys. Heat Transfer **8**, 236 (1994).
[21] E. Josyula, *Hypersonic Nonequilibrium Flows: Fundamentals and Recent Advances* (AIAA, Reston, VA, 2015).
[22] C. Park, *Nonequilibrium Hypersonic Aerothermodynamics* (Wiley, New York, 1990).
[23] R. C. Millikan and D. R. White, Systematics of vibrational relaxation, J. Chem. Phys. **39**, 3209 (1963).
[24] C. Park, Review of chemical-kinetic problems of future NASA missions, I: Earth entries, J. Thermophys. Heat Transfer **7**, 385 (1993).
[25] J. Hao, J. Wang, and C. Lee, Assessment of vibration–dissociation coupling models for hypersonic nonequilibrium simulations, Aerosp. Sci. Technol. **67**, 433 (2017).
[26] D. A. Andrienko and I. D. Boyd, Investigation of oxygen vibrational relaxation by quasi-classical trajectory method, Chem. Phys. **459**, 1 (2015).
[27] I. V. Adamovich, S. O. Macheret, J. W. Rich, and C. E. Treanor, Vibrational relaxation and dissociation behind shock waves part 1: Kinetic rate models, AIAA J. **33**, 1064 (1995).
[28] I. V. Adamovich, S. O. Macheret, J. W. Rich, and C. E. Treanor, Vibrational relaxation and dissociation behind shock waves part 2: Master equation modeling, AIAA J. **33**, 1070 (1995).
[29] M. Lino da Silva, J. Loureiro, and V. Guerra, A multiquantum dataset for vibrational excitation and dissociation in high-temperature O_2-O_2 collisions, Chem. Phys. Lett. **531**, 28 (2012).
[30] D. A. Andrienko and I. D. Boyd, Vibrational relaxation and dissociation of oxygen in molecule-atom mixtures, *45th AIAA Thermophysics Conference Dallas, TX, 2015* (AIAA, Reston, VA, 2015).
[31] D. A. Andrienko and I. D. Boyd, Master equation study of vibrational and rotational relaxations of oxygen, J. Thermophys. Heat Transfer **30**, 533 (2016).
[32] L. B. Ibraguimova, A. L. Sergievskaya, V. Yu. Levashov, O. P. Shatalov, Yu. V. Tunik, and I. E. Zabelinskii, Investigation of oxygen dissociation and vibrational relaxation at temperatures 4000–10 800 K, J. Chem. Phys. **139**, 034317 (2013).
[33] D. A. Andrienko and I. D. Boyd, Rovibrational energy transfer and dissociation in O_2-O collisions, J. Chem. Phys. **144**, 104301 (2016).
[34] K. Neitzel, D. Andrienko, and I. D. Boyd, Aerothermochemical nonequilibrium modeling for oxygen flows, J. Thermophys. Heat Transfer **31**, 634 (2017).